Plasmonic sensing: FDTD calculations to interpret experimental LSPR water adsorption isotherms

Benjamin Demirdjian, Igor Ozerov, F. Bedu, Alain Ranguis, Claude R Henry

Plasmonic sensing: FDTD calculations to interpret experimental LSPR water adsorption isotherms.

Benjamin Demirdjian*, Igor Ozerov, Frédéric Bedu, Alain Ranguis, and Claude R. Henry

Aix Marseille Univ, CNRS, CINAM, Marseille, France

*Corresponding author:

B. Demirdjian, Aix-Marseille Univ., CNRS, CINaM UMR 7325, 13288 Marseille, France

mobile: +33 (0)6 6036 2818, fax: +33 (0)4 9141 8916, e-mail: benjamin.demirdjian@cnrs.fr

ABSTRACT

Finite-Difference Time-Domain (FDTD) calculations are widely used to interpret experimental Localized Surface Plasmon Resonance (LSPR) spectra. With FDTD it is possible to predict the physical parameters of the nanostructures that will theoretically give the best experimental LSPR signals. This information is crucial for optimizing sample fabrication and saving significant time. FDTD is also essential to control and calibrate various parameters of the nanostructures and to understand effects such as a Cr adhesion layer and LSPR sensor size distribution. Finally, for water adsorption sensing, FDTD confirms that the LSPR peak shift strictly follows Campbell's model, even at submonolayer coverage.

KEYWORDS: LSPR, FDTD, gold nanoparticles, water adsorption isotherm, plasmonic sensing

1. INTRODUCTION

Finite-Difference Time-Domain (FDTD) calculations are widely used in the literature and allow to compare experimental Localized Surface Plasmon Resonance (LSPR) results with simulated spectra. Grand *et al.* [1] show that the FDTD method can be used as a powerful tool for predicting plasmon resonances of metallic nanoparticles in the UV-Vis spectral region. Tira *et al.* [2] use FDTD simulations to successfully analyze the far- and near- electromagnetic field response of gold nanoparticles organized in chain-like structures as a function of the number of particles and the interparticle distance in the structures. Wang *et al.* [3] present a paradigm for understanding the growth process of nanostructures and predicting their plasmonic properties by combining experiments and theoretical modeling. In addition, FDTD calculations are critical in predicting the nanoparticle parameters (shape, aspect ratio, spacing) that in theory will give the best LSPR signal. Furthermore, it is possible to go further with FDTD and realize inverse design of plasmonic nanostructures [4]. This information is of great value to the nanofabrication platforms, as it saves a lot of time and money by avoiding by avoiding the fabrication of numerous test samples. After fabricating the plasmonic sensor, FDTD is also useful to control and calibrate different parameters of the nanostructures and to understand various effects such as a Cr adhesion layer, and LSPR sensor size distribution. Finally, FDTD calculations are useful to better understand the adsorption of gas molecules on metallic LSPR sensors. More precisely, in an actual sensing experiment, optical detection is achieved when H_2O gas molecules bind to the Au surface, forming an adsorbed water layer. This binding causes a change in the refractive index of the dielectric environment at the gold surface, resulting in a shift in the resonant wavelength of the Au LSPR detector [5]. In our FDTD calculations, we have chosen a mesh size that is fine enough to resolve the material interfaces and the fields near the interfaces for adsorbed water films from submonolayer to multilayer coverage.

In this paper, we will illustrate the power of the FDTD method by a systematic comparison between experimental LSPR data and those calculated by FDTD models. In fact, we have found many purely theoretical or purely experimental works but few papers with a systematic comparison

of both FDTD calculations and LSPR experiments. However, this is essential to verify the FDTD predictions made.

2. FDTD SIMULATIONS: A CRUCIAL TOOL TO OPTIMIZE, CONTROL, AND CALIBRATE THE LSPR SENSOR PARAMETERS.

The modeling tasks were performed by using a commercial Ansys Lumerical FDTD simulation software package [6]. FDTD is a method used to solve Maxwell's equations in complex geometries. As a direct solution in time and space, it offers the user a unique insight into all types of problems in electromagnetic and photonics. In addition, FDTD can also obtain the frequency solution by exploiting Fourier transforms, allowing a full range of useful quantities to be calculated, such as the transmission/reflection of light. The optical constants of the different material constituents are provided by the software material database, which is based on the reference [7]. Fig. 1 shows typical Au nanodisks on a borosilicate glass substrate with dimensions 750 x 750 x 750 nm^3. The computational domain has the following dimensions: 300 nm in the *X* and the *Y* directions and 400 nm in the *Z* direction (Fig. 1). The Au structures are periodic in the *X* and *Y* directions, so periodic boundary conditions (PBC) were applied in these directions to reduce the computational cost. Perfectly Matched Layers (PMLs) were considered in the *Z* direction to avoid unwanted reflections. The optical source was defined as an incident plane wave perpendicular to the surface of the structure (Fig. 1) propagating towards the gold nanodisks in a wavelength range from 350 nm to 900 nm. To obtain the reflectance (*R*) data as a function of wavelength, a monitor covering the entire computational domain was placed over the structure. Transmittance (*T*) data as a function of wavelength were obtained using another monitor covering the entire computational domain and placed symmetrically below the structure. Finally, the absorption (*A*) data were obtained using the following relationship $A = 1 - R - T$.

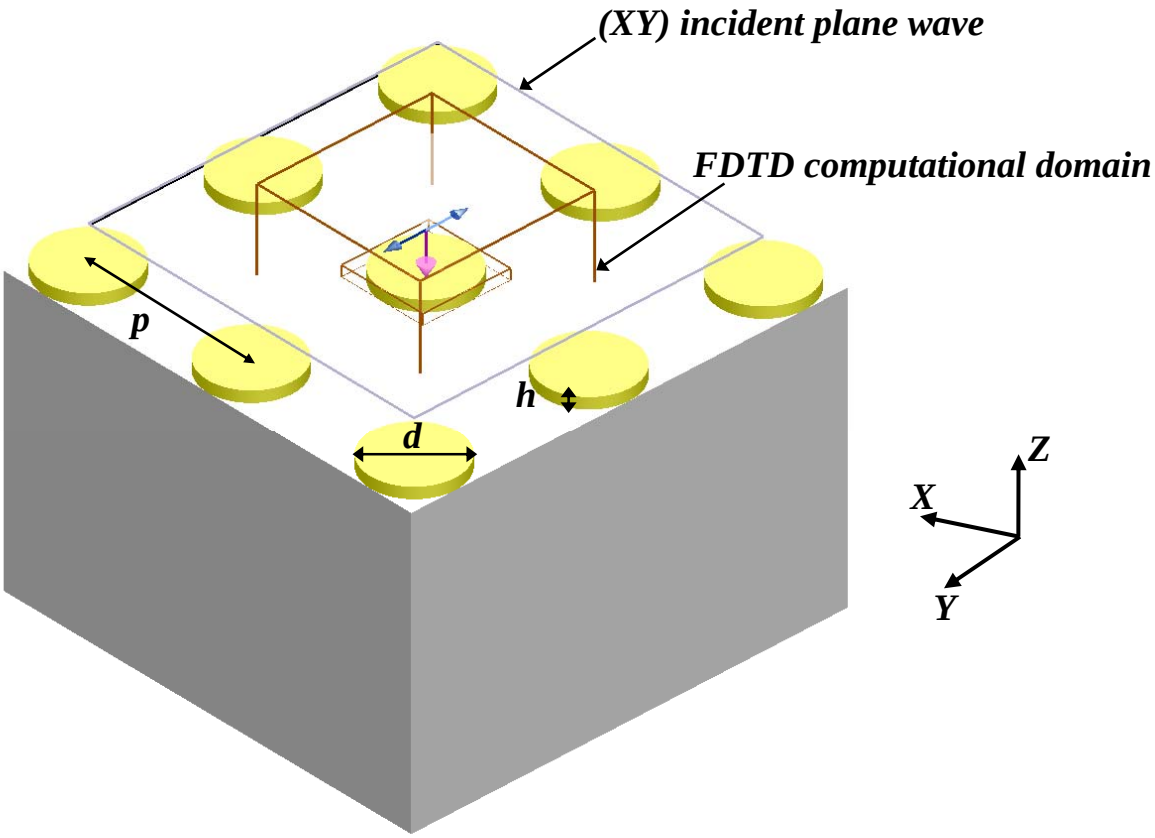

Figure 1: Schematic view of gold nanodisks deposited on a borosilicate glass substrate. The blue arrows indicate the optical source defined as an incident plane wave (XY) perpendicular to the surface of the structure, propagating towards the gold nanodisks (red arrow). The FDTD computational domain is drawn around the central Au disk (300 nm x 300 nm x 400 nm).

FDTD calculations allow us to predict the geometry of the Au disk nanostructures (height *h*, inter-disk distance pitch *p*, diameter *d*) that will theoretically give the best Au LSPR signal. Nanofabrication processes were performed in our laboratory, experimental details can be found in reference [5].

2.1 Effect of the Cr adhesion layer

In order to obtain a good adhesion of the Au disks to the glass substrate during fabrication, it is necessary to sputter or evaporate an adhesion seed layer (usually, chromium or titanium). However, this fact is not always mentioned in the literature. This few nanometer thick metal layer strongly modifies the gold sensor response as it is shown in Fig. 2 for the FDTD simulated LSPR signal.

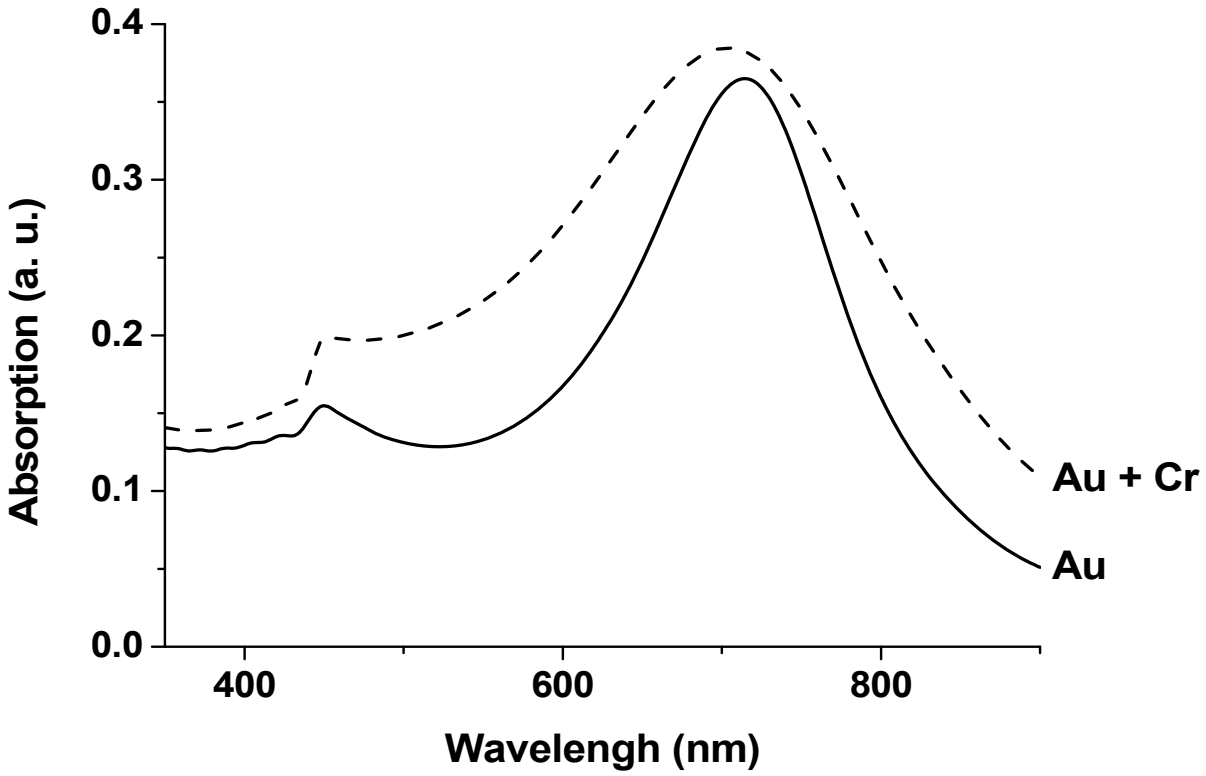

Figure 2: Effect of a 2 nm Cr adhesion layer on the FDTD simulated LSPR ***absorption*** *for Au nanodisks (h = 26 nm, d = 150 nm, p = 300 nm) deposited onto a borosilicate glass window. The solid line corresponds to the bare Au disks, the dashed line corresponds to Au disks with a 2 nm Cr adhesion layer.*

Indeed, comparing Au disks (h = 26 nm, d = 150 nm, p = 300 nm) with (dashed line) and without (solid line) a 2 nm Cr adhesion layer, we observe that the Cr interfacial layer significantly blueshifts the Au LSPR peak position ($\Delta\lambda$ = - 10.2 nm) and broadens its *FWHM* from 105.0 nm to 156.0 nm (Fig. 2). This result is in qualitative agreement with the work of Zheng *et al.* [8]. The Cr layer is optically active in the studied spectral region. It degrades the optical properties of the plasmonic sensor and induces a damping of its resonance.

On the other hand, we have fitted the experimental LSPR signals by FDTD calculations in Fig. 3, where the best-fit parameters are obtained for an Au disks thickness of h = 23.5 nm (d = 150 nm, p = 300 nm) and a Cr layer of 2 nm. The fitting procedure allows us to calibrate both Au and Cr thicknesses with high precision. Experimentally, these thicknesses are measured *in situ* during deposition using a quartz microbalance and then verified using a mechanical contact profilometer.

2.2 Effect of Au disks diameter distribution

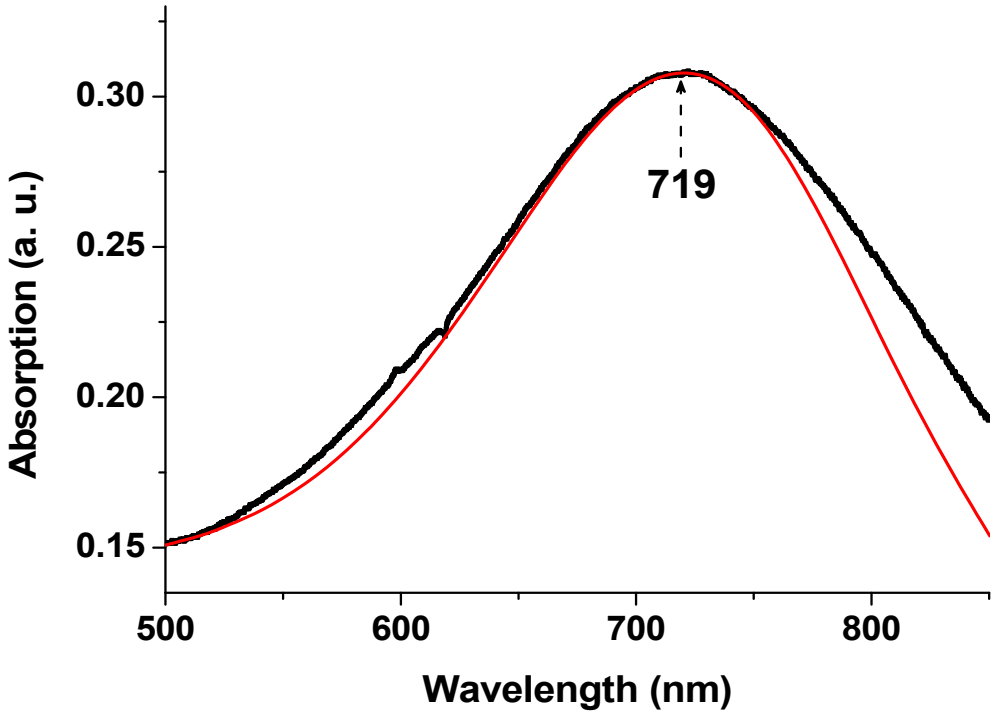

Figure 3: Experimental LSPR ***absorption*** *(black points) for* ***Au*** *nanodisks deposited onto a borosilicate glass window (P_{atm}, RT). The normalized FDTD simulated LSPR response (red solid line) corresponds to Au disks with d = 150 nm, p = 300 nm, h = 23.5 nm and a 2 nm Cr layer.*

In Fig. 3, the fit curve is narrower than the experimental points, especially at longer wavelengths. To explain this phenomenon, we assumed that there is a dispersion of the diameters of the fabricated disks, which is also observed by scanning electron microscopy and atomic force microscopy (Fig. S1). Therefore, we enlarged FDTD computational domain (900 nm in the *X* and *Y* directions, 400 nm in the *Z* direction) and modelled a spectral response of an array of 9 Au disks whose diameters followed a Gaussian size distribution centered on d = 150 nm (Fig. 4). We performed FDTD calculations with this Au disk diameter size distribution and compared it with previous results for an array of homogeneous Au disks with the same diameter d = 150 nm and height h = 23.5 nm.

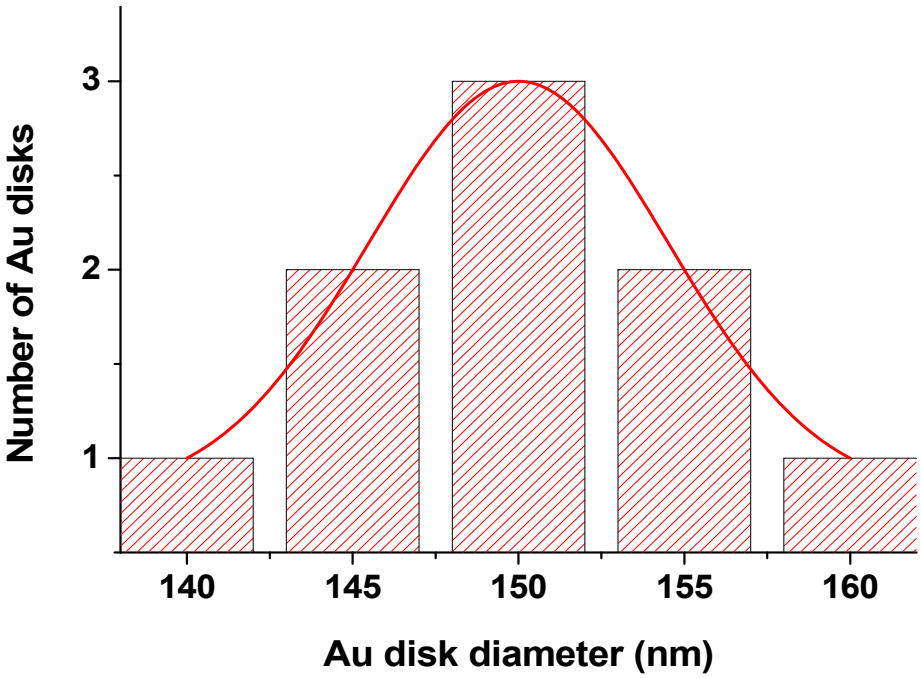

Figure 4: Gaussian Au disks diameter distribution used in the FDTD calculations of Fig. 5.

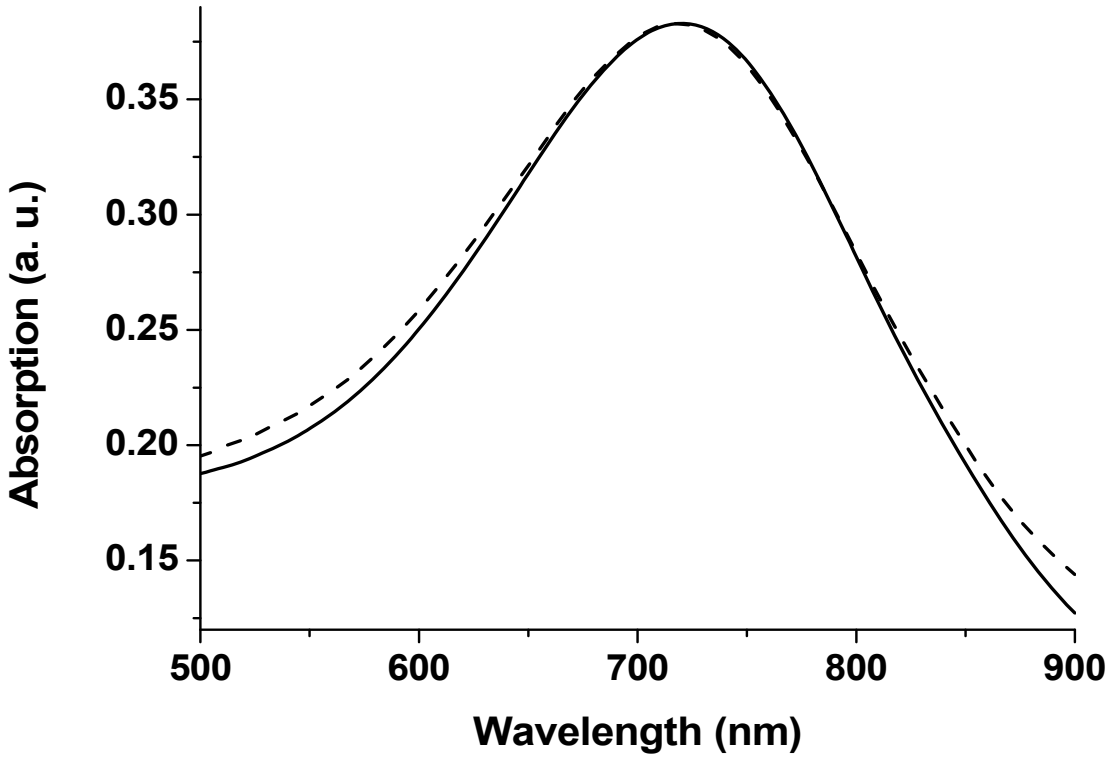

Figure 5: FDTD simulated LSPR absorption corresponding to Au disks (h = 23.5 nm, p = 300 nm) deposited onto a borosilicate glass window. Solid line: d = 150 nm and a 2 nm Cr layer; dashed line: d follows the Gaussian diameter distribution of the Au disks (cf Fig. 4) and a 2 nm Cr layer.

The results presented in Fig. 5 show that the calculated LSPR signal coming from the array with Gaussian Au disk diameter distribution is slightly larger and slightly blue-shifted ($\Delta\lambda$ = - 1.8 nm)

compared to the array of homogeneous diameter disk. This comparison partially explains the result shown in Fig. 3, where the experimental peak is larger than that obtained from FDTD calculations. Fig. 3 also shows an asymmetry and broadening of the LSPR peak already observed in [9] and partly attributed to instrumental noise.

3. FDTD FOR INTERPRETATION OF LSPR WATER ADSORPTION EXPERIMENTS

When molecules are adsorbed on a plasmonic sensor, tiny local changes in the refractive index strongly modify the LSPR response of noble metal nanoparticles [10]. The LSPR response wavelength, corresponding to the absorption maximum is shifted and follows Campbell's model [11]:

$$\Delta\lambda = m\,(n_2-n_1)\,[1 - \exp(\frac{-2d}{l_d})]. \qquad (1)$$

$\Delta\lambda$: LSPR wavelength shift

n_1, n_2: refractive indices varying during adsorption from n_1 (vacuum) to n_2 (condensed phase)

m: refractive index sensitivity.

d: effective thickness of the adsorbed layer

l_d: decay characteristic length of the evanescent electromagnetic field

In surface science, the interaction of water with metal surfaces has been largely studied [12], because H_2O molecules are involved in environmental chemistry, catalysis, biology, material corrosion, and electrochemistry. On gold surfaces, controversies still remain concerning the adsorbed water layer thickness [13-16]. These authors used complementary techniques on single crystal and polycrystalline gold surfaces to measure water layer thicknesses ranging from a single bilayer to several nanometers. In reference [5], we used plasmonic sensing to precisely determine the thickness of the water layer adsorbed on Au nanodisk surfaces. At room temperature, we followed the evolution of the shift $\Delta\lambda$ of the Au LSPR response as a function of the relative humidity (RH %) inside the reactor. At RH = 100 % we measured $\Delta\lambda_{max}$ = 3.95 nm, corresponding

to an adsorbed water layer thickness of d = 1.41 nm *i.e.* 4.7 water monolayers (ML) (Fig. 6), assuming 0.3 nm per monolayer (mean van der Waals diameter of water in [17]). To calculate d (~ water coverage) from equation (1) we used the following experimentally determined parameters: m_{exp} = 163 nm / RIU and ld_{exp} = 37 nm [5].

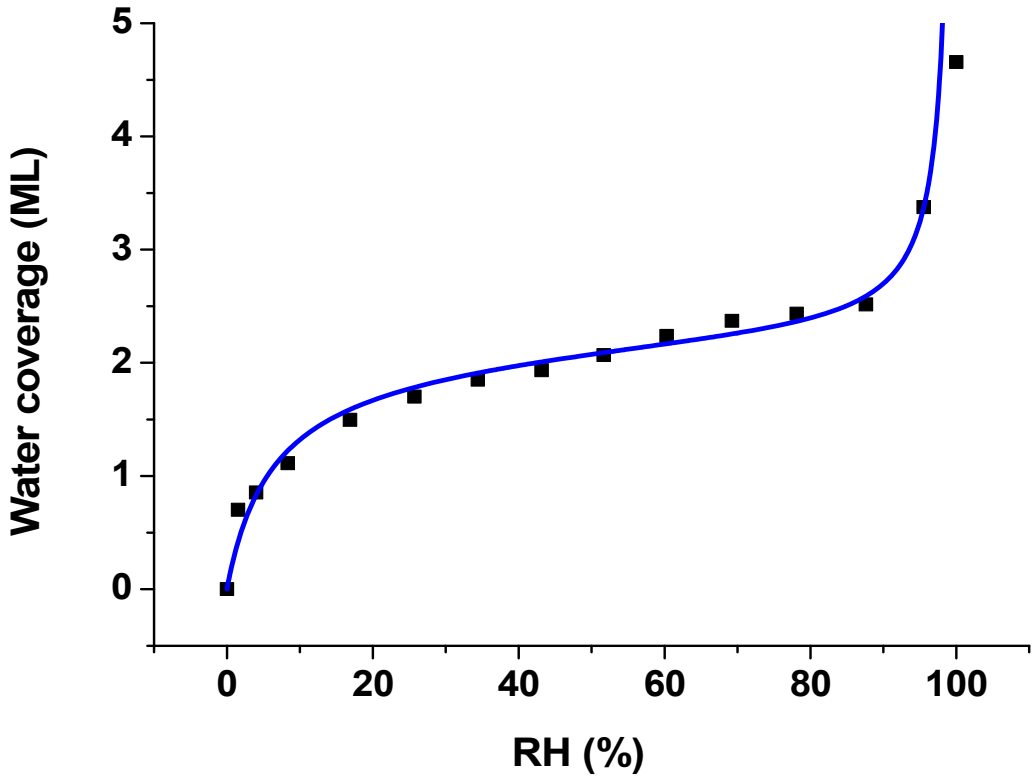

Figure 6: Experimental black points from [5] showing the evolution at RT of the water coverage (resulting from the LSPR shift Δλ) vs the RH inside the reactor during the adsorption of water vapor on bare Au nanodisks (h = 29 nm, p = 300 nm, d = 150 nm) supported onto borosilicate glass windows. The blue curve corresponds to the Pantuso-Tolaba-Aguerre (PTA) model [19], confirming that this curve follows the type II adsorption isotherm model.

Fig. 6 shows the evolution at RT of the water coverage (resulting from the LSPR shift $\Delta\lambda$) as a function of the *RH* inside the reactor during the adsorption of water vapor on bare Au nanodisks (h = 29 nm, p = 300 nm, d = 150 nm) supported on borosilicate glass windows. It was not possible to fit the experimental points with a classical BET model [18]. A good fit (blue curve in Fig. 6) is

obtained using the Pantuso-Tolaba-Aguerre (PTA) adsorption isotherm model presented below [19]. A scaling factor of 1.9 was introduced to correctly adjust the amount of water adsorbed.

PTA model: $$\theta = \left[\frac{\alpha(P/P_0)}{1+(\alpha-1)(P/P_0)}\right]\left[\frac{1-\beta(P/P_0)^{n_1}}{1-(P/P_0)}\right]$$

θ is the surface coverage, P and P_0 are the equilibrium and the saturation pressures of water vapor (at RT), R is the gas constant, β and n_1 are constants determined empirically from the isotherm data and α is the BET constant [18]: $\alpha = \exp[(E_1 - E_L) / RT]$

E_L is the latent heat of condensation of water (40.9 kJ/mol), E_1 is the isosteric heat of adsorption of the first layer. Our fit gives a value for the BET constant $\alpha = 17$, which gives a heat of adsorption for the first layer of $E_1 = 47.9$ kJ/mol. This is close to the experimental values at room temperature obtained by Sharma *et al.* [20] on porous plated gold on copper (45.1 kJ/mol) and by Lee *et al.* [21] on less porous gold-coated AT-cut quartz crystal (44.6 kJ/mol). Theoretical DFT values obtained on Au(111) surface [22] also indicate a value close to our experimental result, in fact they calculated a binding energy of the first layer of 47.3 kJ/mol.

Our fitting results indicate that the adsorption follows a type II adsorption model corresponding to a multilayer physisorption process as in Brião *et al.* [19], Sharma *et al.* [20] and Adolphs *et al.* [23].

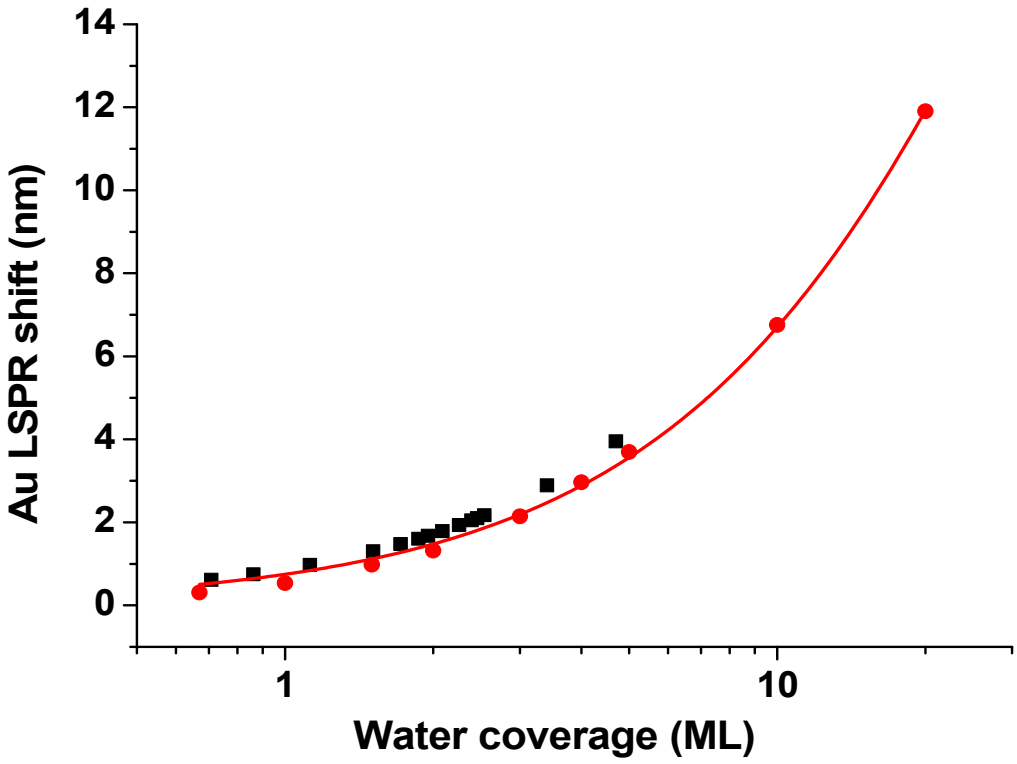

Figure 7: *Au LSPR shifts (Δλ) vs the water coverage for water molecules adsorbed on bare Au disks (h = 29 nm, p = 300 nm, d = 150 nm) supported onto borosilicate glass windows. Experimental black square points from [5]. Theoretical Δλ values coming from several FDTD calculations (red circle points) and their BoxLucas1 fit (red curve).*

Fig. 7 shows the experimental black square points (Au LSPR shift $\Delta\lambda$ *vs* water coverage) measured in [5]. Theoretical $\Delta\lambda$ values coming from several FDTD calculations (red circle points) are also plotted in Fig. 7. We chose an automatic non-uniform mesh generation algorithm, a minimum mesh step of 0.1 nm and mesh overrides for water films on Au disks and on glass substrate of dx = dy = 1 nm and dz = 0.1 nm. These FDTD values are well fitted (red curve of Fig. 7, R^2 = 0.999) by a BoxLucas1 function (y = a [1 - exp(-bx)]) confirming that $\Delta\lambda$ (theoretical) follows Campbell's equation (1), even at low coverage. In these FDTD simulations, we assume that water covers both the Au disks and the glass surface. We obtained from the fit m_{th} = 92 nm / RIU and ld_{th} = 24 nm, but these values are smaller than the experimental values from [5]: m_{exp} = 163 nm / RIU and ld_{exp} = 37 nm. It is important to say that we should rely on the m_{exp} and ld_{exp} values because they have been experimentally determined in our previous work [5]. The difference between experimental and

simulated values can be explained by the fact that the calculations correspond to a perfect water monolayer homogeneously adsorbed on a flat model Au surface without any defect. Guo *et al.* [16] also showed that roughness plays an important role in the amount of water adsorbed. On a polycrystalline Au surface, Gil *et al.* also measured that water accumulates in puddles at the grain boundaries and forms a uniform water layer on terraces [14]. Furthermore, the optical properties of water are considered as liquid bulk (n = 1.33), they are certainly different for very thin films. In Fig. 7, the theoretical values indicate that the $\Delta\lambda$ values, *i.e.* the theoretical water layer thickness (number of monolayers), are slightly inferior to the experimental ones. This is consistent with the fact that we had to introduce a scaling factor in Fig. 6 in order to fit correctly the experimental isotherm curve with the PTA model.

5. CONCLUSION

In this paper, we have demonstrated the power of the FDTD method by attempting to systematically compare LSPR experimental data with FDTD calculations. These simulations are essential not only for the fabrication of optimal LSPR nanostructures, but also for the control and calibration of their properties, allowing the sensor design to be fine-tuned for optimal performance in a specific application. They also give us an expert understanding of the effect of a Cr adhesion layer or the size distribution of LSPR sensors. Finally, regarding the adsorption of water vapor molecules on the Au LSPR nanosensors, our calculations have confirmed that the shift of the LSPR optical absorption peak strictly follows Campbell's model, even at submonolayer coverage.

ACKNOWLEDGMENTS

Nanofabrication processes were performed in the PLANETE cleanroom facility (CINaM, Marseille), a part of Renatech+ French National network.

The authors sincerely thank the laboratory electron microscopy service and its agents (A. Altié and D. Chaudanson) for assisting us in SEM observations.

REFERENCES

[1] J. Grand, P.-M. Adam, A.-S. Grimault, A. Vial, M. Lamy de la Chapelle, J.-L. Bijeon, S. Kostcheev, P. Royer, Optical Extinction Spectroscopy of Oblate, Prolate and Ellipsoid Shaped Gold Nanoparticles: Experiments and Theory, Plasmonics 1 (2006) 135-140. https://doi.org/10.1007/s11468-006-9014-7.

[2] C. Tira, D. Tira, T. Simon, S. Astilean, Finite-Difference Time-Domain (FDTD) design of gold nanoparticle chains with specific surface plasmon resonance, Journal of Molecular Structure 1072 (2014) 137-143. https://doi.org/10.1016/j.molstruc.2014.04.086.

[3] H. Wang, Y. Pu, B. Shan, M. Li, Combining Experiments and Theoretical Modeling To Interrogate the Anisotropic Growth and Structure–Plasmonic Property Relationships of Gold Nanostars, Inorganic Chemistry 58, 18 (2019) 12457-12466. https://doi-org.lama.univ-amu.fr/10.1021.

[4] Z. Zeng, P.K. Venuthurumilli, X. Xu, Inverse Design of Plasmonic Structures with FDTD, ACS Photonics 8, 5 (2021) 1489-1496. https://doi.org/10.1021/acsphotonics.1c00260.

[5] B. Demirdjian, F. Bedu, A. Ranguis, I. Ozerov, C.R. Henry, Water Adsorption by a Sensitive Calibrated Gold Plasmonic Nanosensor, Langmuir 34 (2018) 5381-5385. https://doi.org/10.1021/acs.langmuir.8b00040.

[6] Lumerical Solutions Inc. https://optics.ansys.com/hc/en-us/articles/360034914633-Finite-Difference-Time-Domain-FDTD-solver-introduction, 2017 (accessed November 3, 2023).

[7] E.D. Palik, Handbook of Optical Constants of Solids, 1st ed., Academic Press, Maryland, 1991.

[8] Y.B. Zheng, B.K. Juluri, X. Mao, T.R. Walker, T.J. Huang, 2008. Systematic investigation of localized surface plasmon resonance of long-range ordered Au nanodisk arrays. Journal of Applied Physics. 103, 014308. https://doi.org/10.1063/1.2828146.

[9] H.B. Jeon , P.V. Tsalu, J.W. Ha, 2019. Shape Effect on the Refractive Index Sensitivity at Localized Surface Plasmon Resonance Inflection Points of Single Gold Nanocubes with Vertices. Scientific Reports. 9, 13635. https://doi.org/10.1038/s41598-019-50032-3.

[10] M. Soler, L.M. Lechuga, 2021. Principles, Technologies, and Applications of Plasmonic Biosensors. Journal of Applied Physics. 129, 111102. https://doi.org/10.1063/5.0042811.

[11] L.S. Jung, C.T. Campbell, T.M. Chinowsky, M.N. Mar, S.S. Yee, Quantitative interpretation of the response of surface plasmon resonance sensors to adsorbed films, Langmuir 14 (1998) 5636-5648. https://doi.org/10.1021/la971228b.

[12] M.A. Henderson, The interaction of water with solid surfaces: fundamental aspects revisited, Surface Science Reports 46 (2002) 1-308. https://doi.org/10.1016/S0167-5729(01)00020-6.

[13] M.A. Van Spronsen, K.-J. Weststrate, A. Den Dunnen, M.E. Van Reijzen, C. Hahn, L.B.F. Juurlink, Hydrophilic Interaction Between Low-Coordinated Au and Water: H_2O/Au(310) Studied with TPD and XPS, The Journal of Physical Chemistry C 120, 16 (2016) 8693-8703. https://doi.org/10.1021/acs.jpcc.6b00912.

[14] A. Gil, J. Colchero, J. Gómez-Herrero, A.M. Baró, Macroscopic water deposits on polycrystalline gold measured by scanning force microscopy, Ultramicroscopy 86, 1-2 (2001) 1-9. https://doi.org/10.1016/s0304-3991(00)00110-8.

[15] J.M. Heras, E.V. Albano, Adsorption of Water on Gold Films. A Work Function and Thermal Desorption Mass Spectrometry Study, Zeitschrift für Physikalische Chemie 129 (1982) 11-20. https://doi.org/10.1524/zpch.1982.129.1.011.

[16] L.Q. Guo, X.M. Zhao, Y. Bai, L.J. Qiao, Water adsorption behavior on metal surfaces and its influence on surface potential studied by SPM, Applied Surface Science 258, 22 (2012) 9087-9091. https://doi.org/10.1016/j.apsusc.2012.06.003.

[17] F. Franks, Water: 2nd Edition A matrix of life, Royal Society of Chemistry, Cambridge, 2000.

[18] S. Brunauer, P.H. Emmett, E. Teller, Adsorption of Gases in Multimolecular Layers, Journal of the American Chemical Society 60 (1938) 309-319. http://dx.doi.org/10.1021/ja01269a023.

[19] G. de Vargas Brião, M.G.C. da Silva, M.G.A. Vieira, K.H. Chu, 2022. Correlation of type II adsorption isotherms of water contaminants using modified BET equations. Colloid and Interface Science Communications. 46, Article 100557. https://doi.org/10.1016/j.colcom.2021.100557.

[20] S.P. Sharma, J.H. Thomas III, Adsorption of water vapor on thin-gold electroplate on copper, Journal of Vacuum Science and Technology 14 (3), (1977) 825-827. https://doi.org/10.1116/1.569277.

[21] S. Lee, R.W. Staehle, Adsorption Study of Water on Gold Using the Quartz-crystal Microbalance technique: Assessment of BET and FHH Models of Adsorption, International Journal of Materials Research 88, 11 (1997) 880-886. https://doi.org/10.3139/ijmr-1997-0162.

[22] A. Huzayyin, F. Dawson, Analysis of interfacial water multilayers on Au(111) surface, Journal of Electroanalytical Chemistry 748 (2015) 8-15. https://doi.org/10.1016/j.jelechem.2015.04.014.

[23] J. Adolphs, M.J. Setzer, Energetic Classification of Adsorption Isotherms, Journal of Colloid and Interface Science 184 (1996) 443-448. https://doi.org/10.1006/jcis.1996.0639.